SEDIMENTOLOGY the journal of the International Association of Sedimentologists

Sedimentology (2015) **62**, 1184–1197 doi: 10.1111/sed.12183

The evaluation of macroscopic and microscopic textures of sand grains using elliptic Fourier and principal component analysis: Implications for the discrimination of sedimentary environments

KEITA SUZUKI*, HAJIME FUJIWARA* and TOHRU OHTA†
**Graduate School of Creative Science and Engineering, Waseda University, 3-4-1, Ohkubo, Shinjuku-ku, Tokyo 169-8550, Japan (E-mail: dnvtk@moegi.waseda.jp)*
†Faculty of Education and Integrated Arts and Sciences, Waseda University, 1-6-1, Nishiwaseda, Shinjuku-ku, Tokyo 169-8050, Japan

ABSTRACT

A method that integrates elliptic Fourier and principal component analysis is a new development in the analysis of the shapes of sand grains. However, conventional elliptic Fourier and principal component analysis based on the variance–covariance matrix of the elliptic Fourier results can determine only the form of sand grains, and fails to quantify fine-scale boundary smoothness of grains. In this study, sand grains from glacial, fluvial, foreshore and aeolian environments were analysed using both elliptic Fourier and principal component analysis and an extension of elliptic Fourier and principal component analysis based on the correlation matrix to extract information on grain form (macroscopic) and grain boundary smoothness (microscopic) separately. Conventional elliptic Fourier and principal component analysis based on the variance–covariance matrix produces macroscopic particle shape descriptors, such as the elongation index and bump indices. These indices indicate that sand grains exposed to subaqueous transportation (fluvial and foreshore) have forms that are more elongated than those exposed to subaerial transportation (aeolian dunes). However, elliptic Fourier and principal component analysis based on the correlation matrix is, in addition, able to extract microscopic particle features, which can be interpreted in terms of a boundary smoothness index. The boundary smoothness index indicates that the surfaces of glacial grains are the most rugged, whereas the surfaces of aeolian grains are the smoothest. On bivariate plots of the boundary smoothness and elongation indices, samples from fluvial, foreshore, aeolian and glacial environments cluster in discrete regions. In addition, the analysis reveals that glacial grains are exposed to different morphological maturation pathways than those from fluvial, foreshore and aeolian environments.

Keywords Elliptic Fourier, grain shape, principal component analysis, sedimentary environment discrimination.

INTRODUCTION

Investigations of the shapes of clastic sedimentary grains have long been pursued because shape possesses important information regarding the conditions and processes of the hydrodynamic transport and deposition of grains in different sedimentary environments (e.g. Wentworth, 1919; Wadell, 1932, 1933). Methods to quantify the shapes of grains have included the

use of the Krumbein silhouette chart (Krumbein, 1941), roundness and sphericity indices (Wadell, 1932) and angularity indices (Lees, 1964). These approaches have revealed that the overall form and surface smoothness of clastic grains retains fundamental information regarding the environments of sediment transport and deposition. However, objective and quantitative characterization of natural grain form and smoothness remain challenging (e.g. Blott & Pye, 2008; Tafesse *et al.*, 2013).

Fourier analysis has been applied by some authors to quantitatively describe grain shape, and these works revealed that Fourier analyses can effectively characterize the overall form (Schwarcz & Shane, 1969; Dowdeswell, 1982; Thomas *et al.*, 1995) and surface smoothness (Diepenbroek *et al.*, 1992; Kennedy & Lin, 1992) of sedimentary grains. Sedimentological applications of Fourier analysis include the discrimination of depositional environments (Brown *et al.*, 1980; Barclay & Buckingham, 2009; Livsey *et al.*, 2013), provenance analysis (Ehrich *et al.*, 1980; Hudson & Ehrlich, 1980; Mazzullo & Magenheimer, 1987), and the analysis of the weathering history of grains (Pye & Mazzullo, 1994). However, the simultaneous quantification of both grain form and surface smoothness using Fourier analysis has not yet been accomplished, partly because of the difficulties in handling the numerous descriptors that Fourier series expansion produces. Therefore, most previous studies have evaluated selected Fourier descriptors individually and, as a consequence, it has been difficult to speculate on the overall sedimentological significance of the complete set of Fourier analytical results. To obtain descriptions of both grain form and boundary smoothness, it is necessary to collectively quantify the entire sequence of Fourier descriptors; this can be accomplished by using multivariate statistics.

To obtain a multivariate statistical description of Fourier shape descriptors, a combined elliptic Fourier and principal component analysis (EF–PCA) approach has been adopted (e.g. Rohlf & Archie, 1984; Iwata *et al.*, 1998; Rajaei *et al.*, 2014). Recently, Suzuki *et al.* (2013) applied the EF–PCA method to analyse sand grain shapes, revealing some new indices that measure both the degree of grain elongation and the presence of bumps. However, Suzuki *et al.* (2013), which applied conventional EF–PCA, failed to extract boundary smoothness information, which is an important proxy used to represent and characterize sedimentological environments (e.g. Ehrich *et al.*, 1980; Livsey *et al.*, 2013; Suzuki *et al.*, 2013). Here, an extension of Suzuki *et al.* (2013) is developed to extract information on both grain form and boundary smoothness.

SAMPLING SITES

Sand grains from the glacial, fluvial, foreshore and aeolian environments listed in Table 1 were analysed. At each of the eight sites, 3 to 12 sampling locations were selected (Table 2), and 15 particles per sampling location were obtained for the analysis. In total, 720 grains were investigated.

To minimize grain shape variations related to the lithologies of source rocks, samples were collected from systems with granitic source provenances, with the exception of samples from the Athabasca Glacier and the Gobi Desert which contain clasts derived from sedimentary rocks. Below, each sampling site is described briefly.

Glacial samples were collected from the Damma and Athabasca glaciers (Table 1). On the Damma Glacier, which is situated in south-central Switzerland, samples were obtained from inside two moraines deposited in 1927 and 1992 (Bernasconi & BigLink Project Members, 2008). These samples experienced glacial transport at least until 1927 and 1992, respectively. The Athabasca Glacier is located in the Columbia Icefield in the Canadian Rocky Mountains. According to the formation ages of moraines (Luckman, 1988), samples G2-1 to G2-4 underwent glacial transport until 1992 and sample G2-5 underwent glacial transport until 1982.

Fluvial sediments were collected from the Tamashima and Takase rivers, Japan (Fig. 1, Table 1). The Tamashima River is 15 km long and has an average gradient of 2·6%. Sediments were collected from the mouth of the river up to 9 km upstream, at 1·0 to 1·5 km intervals. The Takase River is 45 km in length and has an average gradient of 1·4%; samples were collected from the mouth of the river up to 25 km upstream (Suzuki *et al.*, 2013). Samples FL1-1 and FL2-1 were collected from the uppermost reaches of the Tamashima and Takase rivers, respectively.

Foreshore sediments were collected from the Karatsu and Ukedo areas, Japan (Fig. 1, Table 1). The Karatsu foreshore is located in the inner bay of the Genkai Sea, whereas the Ukedo foreshore faces the Pacific Ocean (Fig. 1). The average fetch lengths of the Karatsu and Ukedo foreshores, as measured using the method of Keddy (1982), are 9·25 km and 200 km, respectively.

Table 1. Summary of sampling locations.

Environment	Locality (abbreviation)	Number of samples	Latitude and longitude	Lithology of source rocks
Glacial	Damma Glacier, Switzerland (G1)*	4	N 46°38′10″– 46°38′20″ E 8°27′38″ – 08°27′48″	Granite
	Athabasca Glacier, Canada (G2)	5	N 52°12′24″ – 52°12′30″ W 117°13′49″ – 117°13′56″	Sedimentary rock
Fluvial	Tamashima River, Japan (FL1)	6	N 33°26′24″ – 33°27′10″ E 130°02′51″ – 130°06′51″	Granite
	Takase River, Japan (FL2)*	12	N 37°28′00″ – 37°29′25″ E 140°55′51″ – 141°00′21″	Granite
Foreshore	Karatsu foreshore, Japan (FO1)	3	N 33°27′12″ – 33°27′18″ E 130°02′19″ – 130°2′22″	Granite
	Ukedo foreshore, Japan (FO2)*	6	N 37°28′15″ – 37°29′28″ E 141°02′12″ – 141°02′29″	Granite
Aeolian	Gobi Desert, Mongolia (A1)	7	N 44°13′33″ – 45°46′13″ E 103°18′46″ – 109°57′47″	Sedimentary rock and granite
	Junggar Desert, China (A2)	4	N 44°42′06″ – 44°42′11″ E 86°14′02″ – 86°14′04″	Granite

*G1, FL2 and FO2 are samples reported by Suzuki *et al.* (2013).

Also, averaged annual maximum wind velocities in the Karatsu and Ukedo foreshores are 11·8 and 14·2 (m sec^{-1}), respectively. Therefore, wave energy is higher in the Ukedo foreshore.

Aeolian sand grain samples were collected from aeolian dunes developed in the Gobi Desert and the Junggar basin (Table 1). The Gobi Desert is a rocky desert extending from northern and north-western China to southern Mongolia. The Junggar basin is located in north-western China. Currently, the Junggar basin is undergoing afforestation, but the area still belongs to a desert to steppe climatic zone.

MATERIALS AND METHODS

The sample preparation and analytical methods used in this study are extensions of those described in Suzuki *et al.* (2013). Collected sands were washed in water and dried, following which medium-sized (200 to 355 μm) sand grains were collected by sieving. Grains of different sizes and mineralogies can experience different physicochemical conditions during transportation and abrasion. Therefore, the quartz grain of 250 to 355 μm size was used for the following reasons. Firstly, as Rogers *et al.* (1963) noted, quartz particles smaller than 200 μm are unlikely to experience abrasion and grinding actions and, therefore, grains smaller than medium-sized barely retain the shapes and boundary smoothness properties attributed to the various sedimentary environments. In addition, statistically sufficient numbers of quartz grains larger than those of medium grain size are difficult to collect, especially in foreshore and aeolian environments.

A digital stereomicroscope (KH-7700; Hirox Co., Tokyo, Japan) was used in this study to capture the digital images of sand grains. The two-dimensional images obtained are projections parallel to the longest and intermediate axes of the grains, because the grain images were captured after settlement on the microscope stage, in which case the shortest axis was perpendicular to the obtained image. Grain images were digitized at a magnification ratio of 200 and stored as 1000 × 1000 pixel images. The digitized images were then binarized (Fig. 2).

Elliptic Fourier and principal component analysis

Previous studies that have used Fourier techniques to analyse grain shape have applied different Fourier expansion methods, such as the use of deviations between calculated and observed radii obtained from the outlines of grains (Schwarcz & Shane, 1969) and Fourier

Table 2. Summary statistics of each index.

	REF1		REF2		REF3		SEF	
Sample ID	Med.	SD	Med.	SD	Med.	SD	Med.	SD
Glacial								
G1-01	0·091	0·150	0·032	0·036	0·052	0·046	−7·477	4·437
G1-02	0·054	0·157	0·048	0·036	0·022	0·049	−11·200	6·282
G1-03	0·055	0·096	0·052	0·034	0·031	0·048	−9·574	4·046
G1-04	0·041	0·119	0·041	0·030	0·030	0·049	−10·537	3·729
G2-01	0·001	0·081	0·037	0·030	0·044	0·028	−3·778	3·889
G2-02	0·062	0·076	0·040	0·034	0·042	0·044	−8·699	3·858
G2-03	0·085	0·108	0·044	0·028	0·039	0·028	−2·418	3·519
G2-04	0·068	0·074	0·027	0·018	0·041	0·025	−3·640	2·339
G2-05	0·084	0·103	0·029	0·038	0·040	0·040	−6·959	4·359
Fluvial								
FL1-01	−0·109	0·130	0·031	0·053	0·033	0·040	−3·428	4·324
FL1-02	−0·120	0·095	0·073	0·046	0·048	0·039	−2·273	3·026
FL1-03	−0·010	0·146	0·046	0·033	0·088	0·045	−2·157	2·466
FL1-04	−0·050	0·119	0·030	0·041	0·032	0·039	−2·227	3·586
FL1-05	−0·016	0·120	0·049	0·030	0·038	0·019	−2·874	3·260
FL1-06	−0·081	0·091	0·050	0·048	0·042	0·039	−4·043	4·202
FL2-01	−0·065	0·148	0·036	0·020	0·035	0·036	0·298	3·757
FL2-02	0·009	0·146	0·063	0·042	0·065	0·041	−2·934	4·442
FL2-03	−0·133	0·108	0·052	0·050	0·043	0·051	−1·618	3·672
FL2-04	−0·025	0·112	0·053	0·041	0·040	0·043	−0·873	4·216
FL2-05	−0·026	0·115	0·050	0·044	0·079	0·043	−4·570	2·529
FL2-06	−0·098	0·162	0·044	0·030	0·054	0·052	−0·976	4·263
FL2-07	−0·067	0·120	0·039	0·039	0·063	0·041	1·014	3·062
FL2-08	−0·073	0·132	0·042	0·046	0·060	0·049	−1·860	3·475
FL2-09	−0·024	0·101	0·046	0·041	0·073	0·050	−2·105	4·514
FL2-10	−0·059	0·143	0·066	0·049	0·046	0·040	−1·691	3·754
FL2-11	0·026	0·117	0·050	0·040	0·032	0·031	−0·321	4·134
FL2-12	−0·004	0·076	0·096	0·065	0·052	0·034	−3·760	2·925
Foreshore								
FO1-01	−0·005	0·161	0·013	0·039	0·052	0·032	−0·939	4·828
FO1-02	0·005	0·131	0·033	0·052	0·028	0·027	−2·531	3·633
FO1-03	−0·131	0·122	0·021	0·033	0·055	0·079	0·186	3·750
FO2-01	0·005	0·132	0·062	0·046	0·027	0·025	2·990	3·159
FO2-02	0·071	0·137	0·046	0·030	0·027	0·024	3·567	3·116
FO2-03	−0·036	0·135	0·055	0·054	0·030	0·054	4·654	2·727
FO2-04	−0·017	0·109	0·068	0·049	0·036	0·037	4·795	2·313
FO2-05	−0·001	0·171	0·043	0·040	0·034	0·032	3·931	3·953
FO2-06	0·015	0·115	0·046	0·064	0·031	0·039	3·329	2·385
FO2-07	0·003	0·111	0·032	0·030	0·015	0·034	4·436	2·402
Aeolian								
A1-01	0·022	0·099	0·030	0·032	0·043	0·028	6·621	2·215
A1-02	0·087	0·092	0·026	0·044	0·027	0·038	2·274	4·058
A1-03	−0·004	0·076	0·040	0·034	0·028	0·035	8·833	2·835
A1-04	0·078	0·099	0·026	0·023	0·035	0·024	10·463	1·331
A1-05	0·071	0·091	0·037	0·025	0·037	0·040	7·908	1·454
A1-06	0·072	0·091	0·058	0·029	0·035	0·027	8·669	2·161
A1-07	0·098	0·081	0·016	0·032	0·025	0·031	6·477	1·893
A2-01	0·083	0·070	0·034	0·037	0·030	0·038	7·352	1·813
A2-02	0·087	0·088	0·038	0·026	0·037	0·034	7·343	2·485
A2-03	0·116	0·103	0·042	0·036	0·044	0·027	8·693	2·254
A2-04	0·083	0·085	0·030	0·031	0·044	0·041	7·144	1·600

Med., median; SD, standard deviation.

amplitude spectra (Ehrlich & Weinberg, 1970). In contrast, Suzuki *et al.* (2013) applied conventional elliptic Fourier analysis (described below) because this method is more suitable for the analysis of grain shape. Firstly, as noted by Boggs (2009), Fourier analyses using the values of radius changes from a grain centre cannot be applied to highly complex shapes, because when grains contain highly convex or concave forms, two or more radial projections might exist for a given central angle. In contrast, elliptic Fourier analysis is amenable to the analysis of such complex forms. In addition, grain form characteristics captured by elliptic Fourier analysis can be reproduced both mathematically and graphically. Therefore, the sedimentological meaning of the results of an elliptic Fourier analysis can be examined visually. For these reasons, elliptic Fourier analysis has been applied widely in the field of biology because it enables the quantification of complex biological forms, such as rootlets, petals and fish skeletons (e.g. Iwata *et al.*, 1998; Yoshioka *et al.*, 2004; Tracey *et al.*, 2006, respectively).

Details regarding the background and methodology of elliptic Fourier analysis can be found in Kuhl & Giardina (1982), Iwata *et al.* (1998) and Iwata & Ukai (2002). The essential points are summarized below and all of these procedures were conducted using the software package SHAPE (Iwata & Ukai, 2002). The outlines of grains are extracted in the form of chain code (Freeman, 1974). Firstly, each grain outline is portrayed as x–y coordinates. Then, the grain outline is traced from an arbitrary point. The projection of traces onto the x and y coordinates would show a periodic oscillation, and the oscillations can be described as a function of frequency revealed by an elliptic Fourier expansion whereby the following two functions are obtained:

$$x(t) = \frac{a_0}{2} + \sum_{n=1}^{N}\left(a_n \cos\frac{2n\pi t}{T} + b_n \sin\frac{2n\pi t}{T}\right)$$

$$y(t) = \frac{c_0}{2} + \sum_{n=1}^{N}\left(c_n \cos\frac{2n\pi t}{T} + d_n \sin\frac{2n\pi t}{T}\right)$$

where t indicates traced distance (unit pixel), a_0 and c_0 are, respectively, the x and y centre coordinates of the traced outline form, n is the harmonic number, N is the total number of harmonics (100 in this study) and T is the perimeter of the grain shape outline. As a result, the properties of the grain form are expressed by a_n, b_n, c_n and d_n (that are called elliptic Fourier descriptors here). In the case of elliptic Fourier spectra of grain shapes, initial and final coordinates are identical and, thus, discontinuity or overall linear trend would not appear. Therefore, spectral filtering such as detrend and taper was not conducted in the present analysis.

The first harmonic (n = 1) was utilized as a normalizing function for the subsequent harmonics; this is because the first harmonic is an elliptic outline of the grain that can be visualized as a projection of the size and orientation of the grain image. Therefore, normalization using this elliptic outline cancels any variations that may be due to the initial position of the grain image, and consistent results can be obtained regardless of the size, azimuth and dislocation of the image. For the pixel size of 1000 × 1000 used in this study, the period of the 100th harmonic is approximately 20 pixels, which corresponds to approximately 1/100 of the perimeter length in the images for this article.

As mentioned above, the most problematic aspect of the Fourier analysis of grain shapes is the number of variables that are returned, which presents difficulties in comprehensively inter-

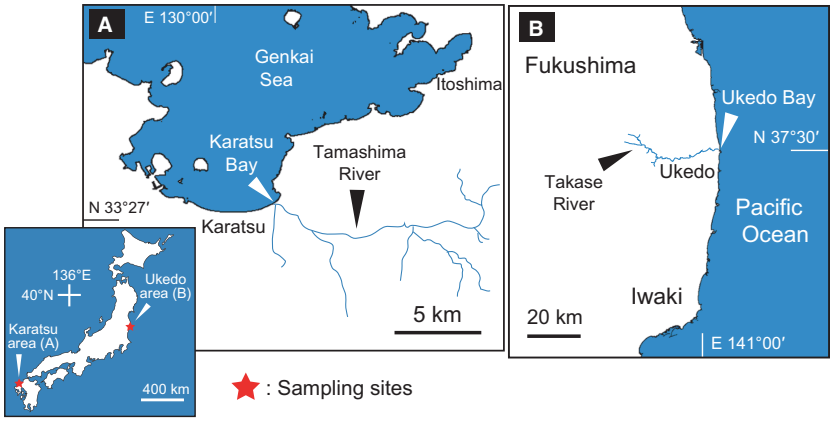

Fig. 1. Locations of sampling sites of fluvial and foreshore sediments. (A) Tamashima River (FL1) and Karatsu foreshore (FO1) and (B) Takase River (FL2) and Ukedo foreshore (FO2). The Karatsu foreshore is located in an inner bay, whereas the Ukedo foreshore faces the Pacific Ocean.

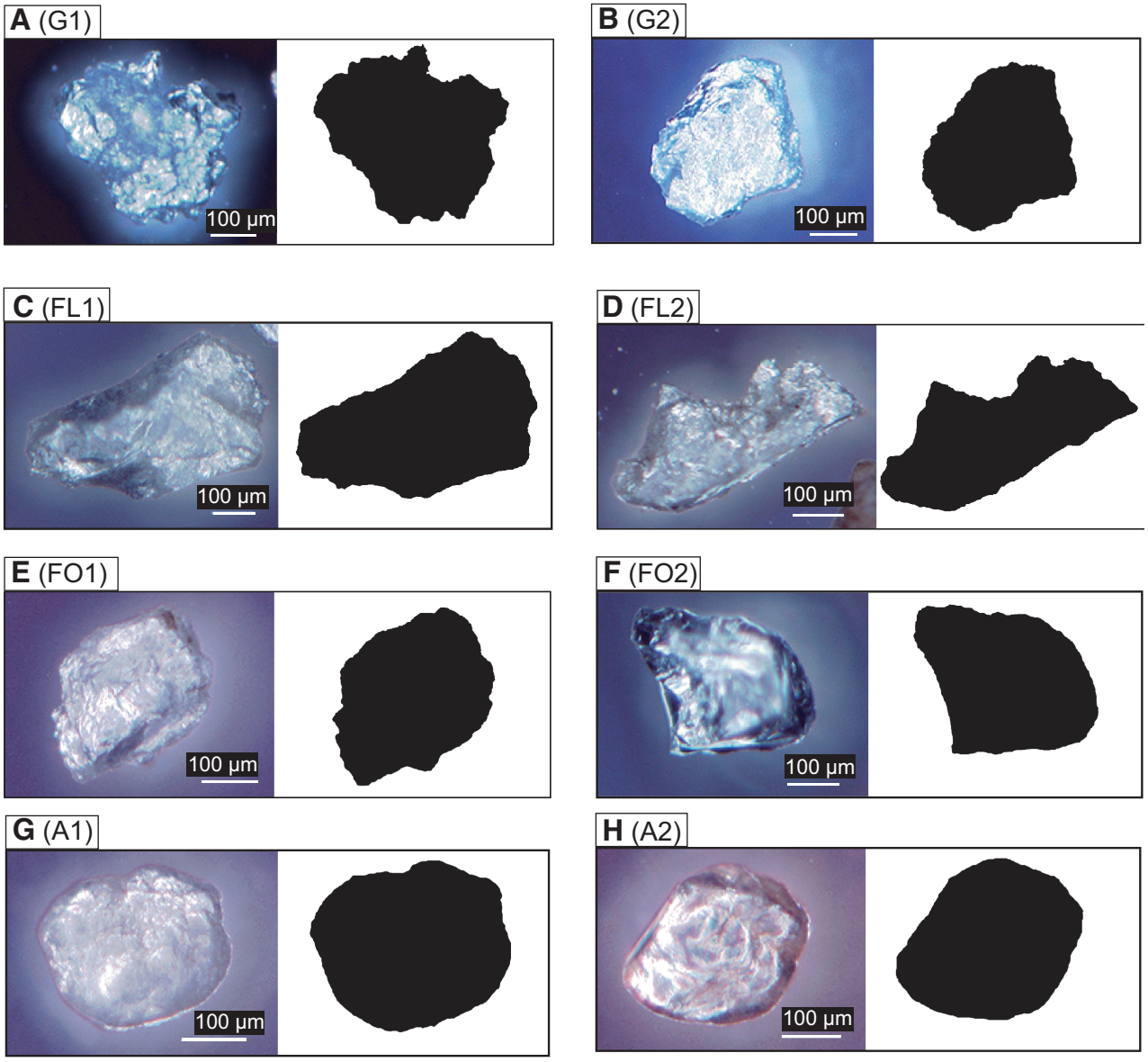

Fig. 2. Representative photographs and binarized images of grains: (A) glacial grain from Damma Glacier (G1); (B) glacial grain from Athabasca Glacier (G2); (C) fluvial grain from Tamashima River (FL1); (D) fluvial grain from Takase River (FL2); (E) foreshore grain from Karatsu foreshore (FO1); (F) foreshore grain from Ukedo foreshore (FO2); (G) aeolian grain from the Gobi Desert (A1); (H) aeolian grain from the Junggar Desert (A2). Samples G1, FL2 and FO2 were reported by Suzuki *et al.* (2013).

preting such large datasets (Boggs, 2009). In the present case, 397 variables were generated for each grain. To overcome this difficulty, the elliptic Fourier results were further analysed using principal component analysis (the EF–PCA method).

To the knowledge of the present authors, all previous EF–PCA studies have conducted PCA based on the variance–covariance matrix deduced from the results of the above EF analysis (e.g. Iwata *et al.*, 1998; Suzuki *et al.*, 2013; Rajaei *et al.*, 2014); however, none of these studies has utilized the correlation matrix. Principal component analysis results are strongly affected by variables with large variances. Because extracted trigonometric functions that contain large amplitudes will generally have large variances, compared with small-amplitude descriptors (Fig. 3A), the grain shape characteristics described by the large-amplitude functions would be preferentially emphasized by the use of non-standardized variance–covariance matrix. The advantage of the

use of the variance–covariance matrix is that the overall form of grains can be depicted; however, the disadvantage is that fine-grained shape characteristics are masked (Suzuki *et al.*, 2013). In contrast, the use of the standardized correlation matrix ensures that the variances of all large-amplitude and small-amplitude descriptors are treated equally (Fig. 3B). Consequently, it is expected that the use of the correlation matrix will preferentially emphasize the contributions of the high-frequency details of grain surface structures compared to overall grain form (Fig. 3B). Therefore, EF–PCA was conducted on both the variance–covariance and correlation matrices in this study.

To conduct the EF–PCA based on the correlation matrix, the amplitudes of each elliptic Fourier descriptors are defined as:

$$x_n = \sqrt{a_n^2 + b_n^2}$$

$$y_n = \sqrt{c_n^2 + d_n^2}$$

Using this approach, the 397 Fourier descriptors (a_n, b_n, c_n, and d_n) were converted into 199 amplitudes (x_n and y_n).

Grain shape indices [the elongation index (REF1) and bump indices (REF2 and REF3), and the boundary smoothness index (SEF, standardized elliptic Fourier)] that will be proposed in the following sections can be calculated for any arbitrary sand grain samples by the following steps. (i) Firstly, conduct Elliptic Fourier analysis to the given grain binary image by using the software SHAPE (Iwata & Ukai, 2002; http://lbm.ab.a.u-tokyo.ac.jp/~iwata/shape/). (ii) Multiply the obtained Fourier descriptors and PCA loadings of the present results, element-wisely. Principal component analysis loading data is provided as a 'Supporting Information' spreadsheet file available online (Data S1). (iii) This file automatically calculates the grain shape indices REF1, REF2, REF3 and SEF from the results produced by the SHAPE program.

A Kruskal–Wallis test was conducted to analyse whether the newly proposed indices adequately discriminate sand grains derived from different environments. If the Kruskal–Wallis test identified significant differences, *post hoc* Scheffe's multiple comparison test (Bohrer, 1967) was performed. Scheffe's multiple comparison test has been chosen because it enables round-robin comparison of each environment.

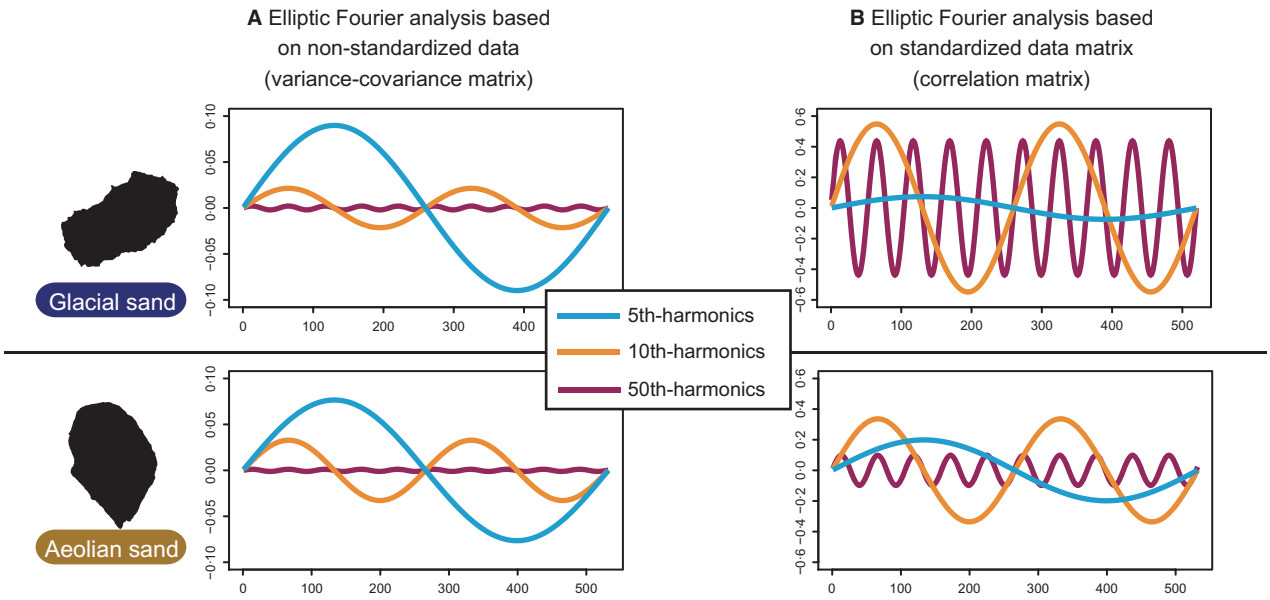

Fig. 3. The relative amplitudes and variances of the 5th, 10th and 50th-elliptic harmonics described by the non-standardized (A) and standardized (B) elliptic Fourier analysis. Grain shape differences described by trigonometric functions with large amplitudes will be emphasized (overall grain shape) by the use of non-standardized data (A). In contrast, the use of standardized data (B) emphasizes small amplitudes (grain boundary smoothness).

RESULTS AND DISCUSSION

Elliptic Fourier and principal component analysis based on the variance–covariance matrix

The results of EF–PCA based on the variance–covariance matrix for 720 quartz sand grains (the 345 quartz grains used by Suzuki *et al.*, 2013; and an additional 375 quartz grains collected for the present study) are compiled and listed in Table 3. Principal components 1 to 3 captured 50·71%, 13·41% and 12·83% of the total variance in the data, respectively (Table 3). These principal components will be referred as REF1, REF2 and REF3 (REF is an abbreviation for Raw Elliptic Fourier), respectively. The grain shape characteristics that each component captures can be described visually (Fig. 4). The idealized images in the centre column of Fig. 4 illustrate grain shape images corresponding to zero values of REF1 to REF3. Images in the right and left columns illustrate grain shapes corresponding to negative and positive scores (at two standard deviations), respectively. According to these images, REF1 can be interpreted as an index of elongation, and REF2 and REF3 quantify the presence of bumps along either the two-dimensionally projected longest axis or the shortest axis, respectively. Although, the number of grains analysed was doubled, the results of the present study are consistent with those of Suzuki *et al.* (2013). This consistency in the pattern across the larger dataset implies that any further addition of grain shape data is not likely to alter the basic elements of the results.

It should be noted that the positive and negative signs of REF2 and REF3 are unimportant and reflect only the mirrorwise positioning of bumps (Fig. 4). Therefore, the absolute values of REF2 and REF3 were used in the following discussions.

The PCA eigenvalues of REF1 to REF3 are tabulated in Table 3, and boxplots of REF1 to REF3 values for each sample derived from different sedimentary environments are shown in Fig. 5. As shown in Fig. 5A, REF1 indices are smallest for fluvial grains, intermediate for foreshore grains, and largest for glacial and aeolian grains. According to the idealized images of grains with varying REF1 indices (Fig. 4), this demonstrates that the degree of elongation differentiates fluvial, foreshore and aeolian grains, but that glacial and aeolian grains retain similar spherical shapes. Also, the Kruskal–Wallis test in Table 4 indicates that REF1 differentiated sand grain groups at a statistically significant confidence level ($P < 0{\cdot}0001$). The multiple comparison test of Scheffe's method was further applied to identify which environmental pairs were actually distinguished by REF1. The results of Table 4 indicate that REF1 differentiates most of the environmental group pairs at a statistically significant confidence level ($P < 0{\cdot}0001$), but the pairs glacier/aeolian and fluvial/foreshore were undifferentiated.

As for the REF2 and REF3 values of aeolian sands, they are somewhat lower than those of other sands; however, the bump indices fail to distinguish between grains in different environ-

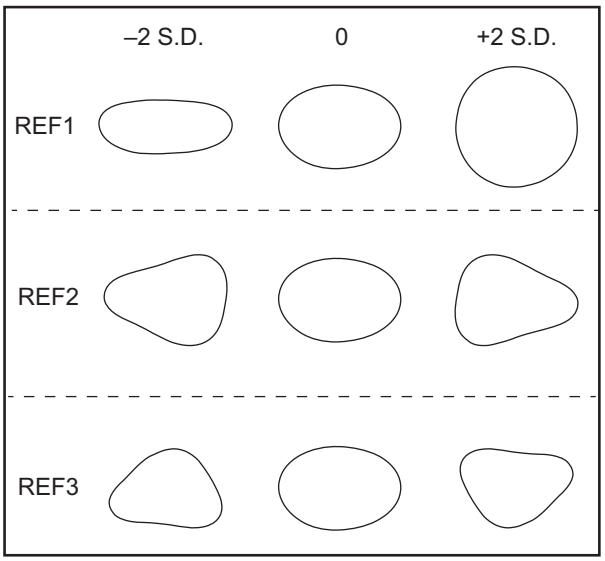

Fig. 4. Idealized images showing the variation in form captured by each principal component (PC), based on results of the principal component analysis (PCA) using the variance–covariance matrix. The middle column of ellipsoidal images shows the form of particles with PC scores of zero, whereas the images in the left and right columns show particles with high and low PC scores (scores plus or minus two times the value of the standard deviation, SD), respectively.

Table 3. Results of PCA based on variance–covariance matrix.

Component	Eigen value (10^{-3})	Proportion (%)	Cumulative (%)
PC1 (REF1)	15·96	50·71	50·71
PC2 (REF2)	4·22	13·41	64·12
PC3 (REF3)	4·04	12·83	76·95

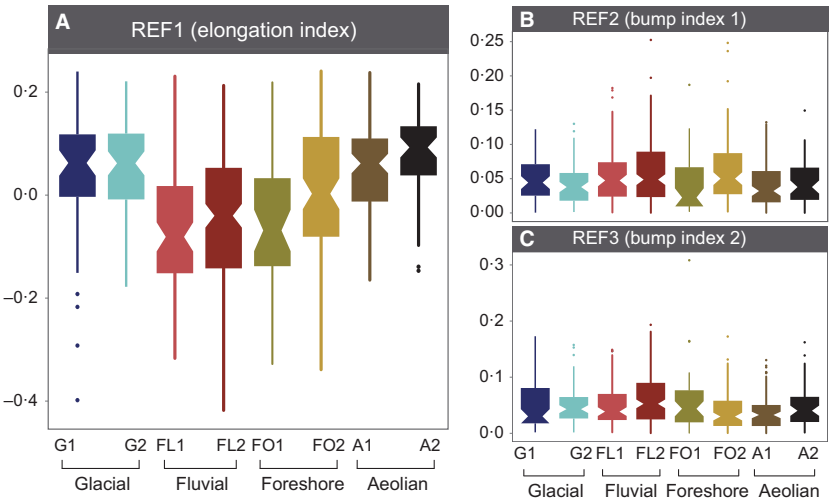

Fig. 5. Boxplots showing variations in the first three principal component scores (REF1, REF2 and REF3) of grains from different sedimentary environments. The lower and upper limits of the each box represent the 1st and 3rd quartiles, respectively, and the line within the box represents the 2nd quartile (median). The widths of notches on the side of each box indicate the 95% confidence interval of the median. Whiskers represent the allowable range of the data (1·5 times of interquartile range). Open circles represent outliers.

Table 4. Multiple comparisons between groups (*P*-values).

	REF1	REF2	REF3	SEF
Kruskal–Wallis test	**<0·0001**	**0·0165**	**0·0017**	**<0·0001**
Scheffe's method for multiple comparison:				
Glacier versus fluvial	**<0·0001**	0·3299	0·5469	**<0·0001**
Glacier versus foreshore	**0·0002**	0·7909	0·6301	**<0·0001**
Glacier versus aeolian	0·8842	0·8561	0·4408	**<0·0001**
Fluvial versus foreshore	0·0588	0·9124	**0·0261**	**<0·0001**
Fluvial versus aeolian	**<0·0001**	**0·0287**	**0·0069**	**<0·0001**
Foreshore versus aeolian	**<0·0001**	0·9926	0·9926	**<0·0001**

P-values that showed statistically significant differences are marked by bold numbers.

ments (Fig. 5B and C). Statistically significant differences were only found between fluvial/aeolian samples for REF2 and fluvial/foreshore and fluvial/aeolian samples for REF3 (Table 4).

In summary, EF–PCA based on the variance–covariance matrix extracts distinguish overall grain form through values of REF1 (the elongation index). The REF1 values indicate that sand grains that have undergone subaqueous transport (fluvial and foreshore) show more elongated forms than do those that have undergone subaerial transport (aeolian), as would be expected from previous work (e.g. Jerolmack & Brzinski, 2010).

However, sands of the Karatsu foreshore (FO1) yield smaller REF1 values than those of Ukedo foreshore sands (FO2), and their values are as small as those of fluvial sands (Fig. 5). The Karatsu foreshore (FO1) is located in an inner bay, whereas the Ukedo foreshore (FO2) faces the open Pacific Ocean (Fig. 1). Both averaged fetch values and wind velocities are consistently smaller in the Karatsu foreshore and, therefore, differences in the wave energy in these fore-

Table 5. Results of PCA based on correlation matrix.

Component	Eigen value	Proportion (%)	Cumulative (%)
PC1 (SEF)	40·71	20·46	20·46
PC2	5·34	2·68	23·14
PC3	3·64	1·83	24·97

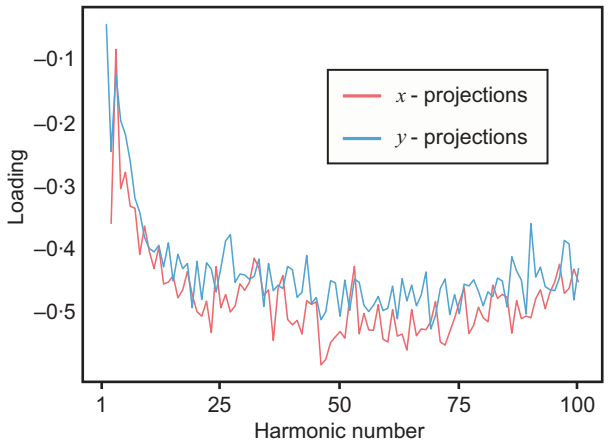

Fig. 6. Loading variations of the first principal component (PC1) of the PCA based on the correlation matrix, showing negative loadings for all harmonics, and especially high negative loadings for harmonics 25 to 100.

shore environments may explain why the values of REF1 are smaller in grains from inner bay foreshore (FO1) and larger in grains from foreshore facing the open ocean (FO2). Consequently, the REF1 values are a potential measure of morphological maturity of the grains.

Elliptic Fourier and principal component analysis based on the correlation matrix

The results of PCA based on the correlation matrix are presented in Table 5. The first principal component (PC1) captures 20·46% of the total variance, and the second principal component (PC2) accounts for 2·68% (Table 5). The proportion of variance explained by PC2 is significantly less than that explained by PC1, indicating that PC2 and the successive principal components are insignificant in terms of describing overall grain morphology. Therefore, only the PC1 output of the EF–PCA based on the correlation matrix was utilized, and is referred to as SEF.

The loadings of each of the harmonics on PC1 are shown in Fig. 6. All of the harmonics show negative loadings, and decrease as the harmonic number increases. The periodicities of harmonic numbers 25 to 100 compared with that of harmonic number 1 (the perimeter of sand particles) are 0·04 to 0·01. Therefore, SEF that has large negative loading values with harmonic numbers 25 to 100, is interpreted as a measure of integrated microscopic boundary smoothness of grains.

Representative binarized grain images that represent the minimum, lower quartile, median, upper quartile and maximum SEF values are shown in Fig. 7A. The SEF values increase with increasing degrees of grain boundary smoothness. These visual inspections confirm the interpretation that SEF is an index of boundary smoothness.

Boxplots of SEF values from grains in different sedimentary environments (Fig. 8) show that aeolian sand grains have the highest values of SEF, followed by foreshore, fluvial and glacial sand grains. As expected, the SEF values indicate that the surfaces of glacial grains are the most rugged, whereas those of aeolian grains are the smoothest. In addition, multiple comparison statistical tests (Table 4) returned significantly low *P*-values for all environment pairs compared, enabling discrimination of all analysed sedimentary environments.

Abrasion rates of grains are a function of particle velocity and particle diameter (Anderson,

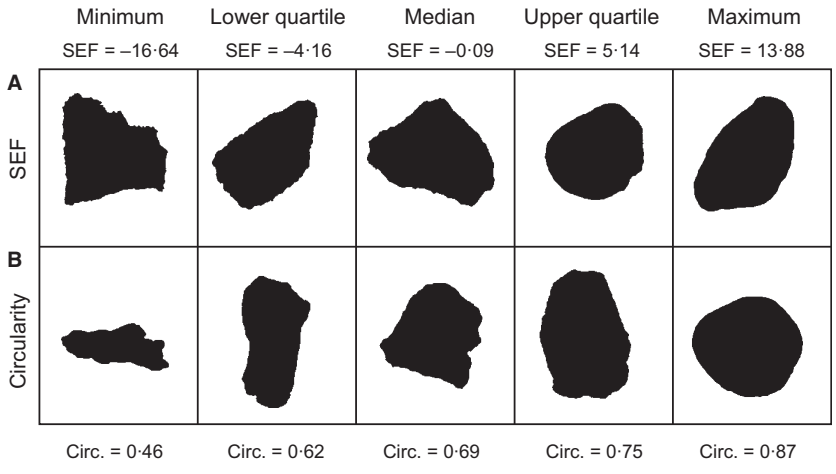

Fig. 7. Selected binarized particle images showing minimum, lower quartile, median, upper quartile and maximum values of the SEF (A) and circularity (B) indices. (A) Increases in grain boundary smoothness are represented by increasing SEF values. (B) Both overall form and boundary smoothness of grains change concordantly with increasing circularity (Circ.) values.

1986; Jerolmack & Brzinski, 2010). Because particle velocities generally increase in the order of glacial, fluvial, foreshore and aeolian environments; and because the SEF values indicate that the particle surface becomes smoother in this order (Fig. 8), the SEF value of a grain can be considered as an index of sediment maturity in a given sedimentary environment.

The only exception to this pattern appears in the foreshore sand samples of FO1 (Fig. 8), which overlap with those of fluvial sands, as in REF1 values (Fig. 5A). The lower wave energy in the Karatsu foreshore (FO1) compared to the Ukedo foreshore (FO2) is the possible reason why Karatsu sands yield SEF values that are as low as those of fluvial sands (Fig. 8). The differences between the SEF values of grains in samples FO1 and FO2 indicate that SEF detected regional variations in foreshore wave power. If the SEF values were truly proportional to foreshore wave intensities, then the SEF index might serve as a proxy for measuring wave power in palaeo-foreshore environments. However, further assessments based on a larger dataset of foreshore sands are necessary.

Comparisons with other shape indices

The REF1 and SEF values were compared with those of the circularity index, which is commonly used as a grain shape parameter (Cox, 1927; Hentschel & Page, 2003; Tysmans *et al.*, 2006). Variations in boxplots of circularity (Fig. 9A) are similar to those of the boxplots representing REF1 values (Fig. 5A), with discrepancies observed in the values of the Damma and Athabasca glacial samples (Fig. 9). However, the REF1 values of these glacial samples are identical (Fig. 5A). Therefore, the differences identified by the circularity index are not only expressed in REF1 values but also in SEF values (Fig. 8).

Variations in boxplots of sums of standardized REF1 and SEF values (Fig. 9B) are very similar in pattern to just circularity (Fig. 9A). Therefore, the grain characteristic that circularity describes is, quantitatively, a combination of form (REF1) and surface smoothness (SEF). This interpretation is confirmed visually in Fig. 7B, which

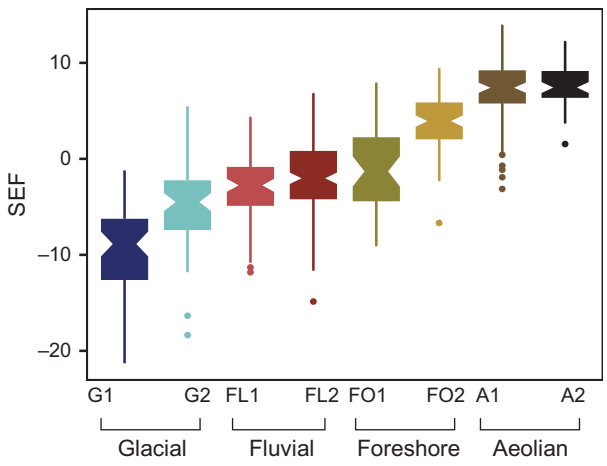

Fig. 8. Boxplots showing variations in SEF values. The surfaces of aeolian grains are the smoothest, whereas the surfaces of glacial grains are rough. Notches in each of the bars (representing 95% confidence intervals around the median value) show that the parameters of grains in sedimentary environments do not overlap, except for those of FO2. See the caption of Fig. 5 for the descriptions of boxplot features.

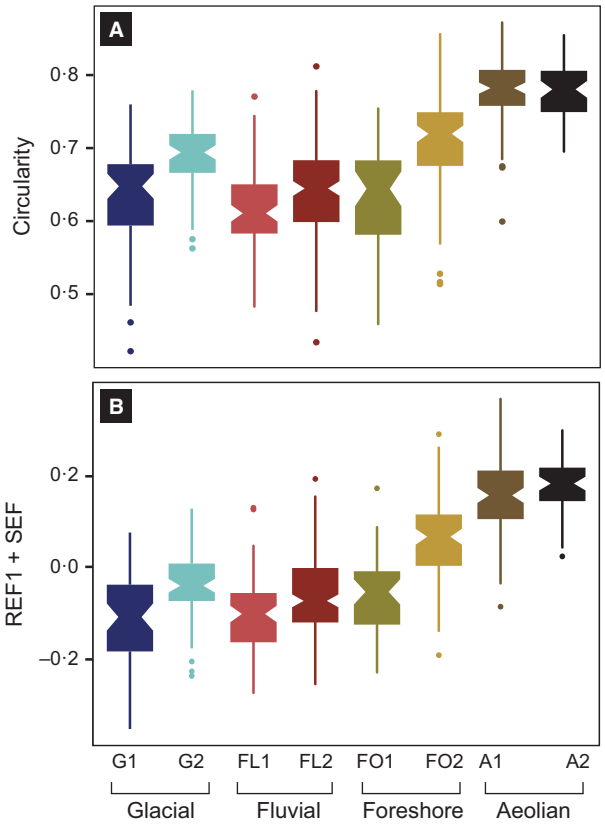

Fig. 9. Boxplots showing variations in the circularity index (A) and REF1 + SEF values (B) of grains in different sedimentary environments. The two boxplots are quantitatively identical, indicating that circularity measures a combination of grain shape parameters, which include those representing overall form and surface smoothness. See the caption of Fig. 5 for the descriptions of boxplot features.

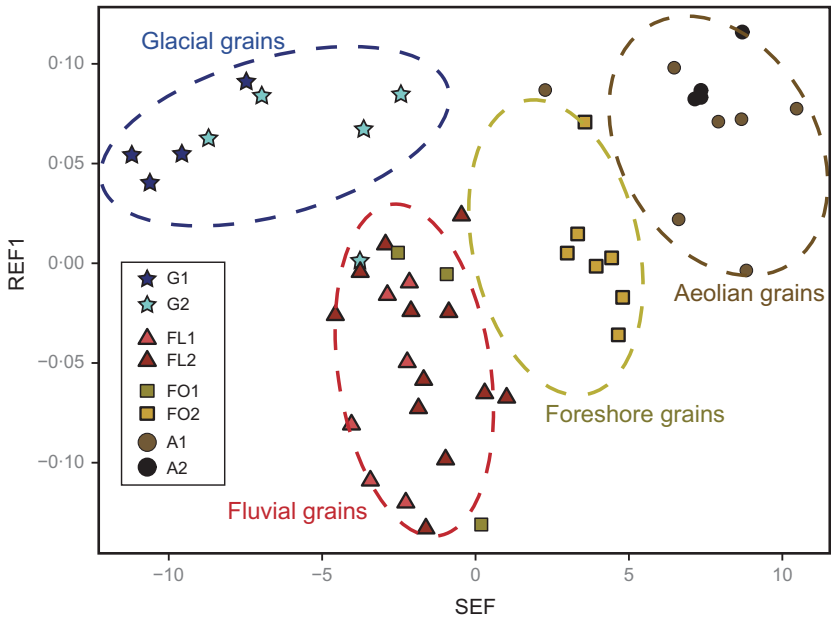

Fig. 10. Scatter plot of REF1 versus SEF median values of individual samples. Grains from the different sedimentary environments plot in distinctive regions. Note the presence of two distinct pathways of the spheronization and abrasion of sediments. The evolutionary pathway of sediment maturity for glacial sediments differs from those for fluvial, foreshore and aeolian sediments.

shows minimum, lower quartile, median, upper quartile and maximum values of circularity. These images demonstrate that circularity values increase as grain surfaces become smoother and overall shapes become rounder. Separation of form (REF1) and boundary smoothness (SEF) is useful but was a difficult task when using conventional indices.

The standardized elliptic Fourier – raw elliptic Fourier diagram

The value of REF1 increases as a grain changes from oblate to spherical, and the value of SEF increases as grains are abraded. The values of the REF1 and SEF indices vary depending on the sedimentological processes affecting the grains. On a SEF–REF1 diagram (Fig. 10), samples from each environment cluster together into discrete regions representing the fluvial, foreshore, aeolian and glacial environments of the grains. When both indices are taken into account, the SEF–REF1 space improves the discriminatory ability of the parameters to characterize sedimentary environments (Fig. 10). Still, samples from the Karatsu foreshore (FO1) do not discriminate from fluvial sands (FL1 and FL2), probably because of the faint wave intensity in Karatsu Bay. For this reason, a further assessment of the reliability of SEF–REF1 diagrams to discriminate between different sedimentary environments is required, because this study considered only two localities for each environment.

Grains transported by fluids, either water or air, define one continuous pathway aligned in an order of fluvial, foreshore and aeolian, which possibly suggests an evolving order of sediment physical maturity (Fig. 10). In fact, foreshore sediments collected from the inner bay (FO1) are located at the initial point of this maturity path, whereas those from the open ocean (FO2) are located at an intermediate position (Fig. 10). Therefore, the degree of morphological maturation can be detected by the use of the REF1–SEF diagram. If SEF–REF1 can truly serve as a proxy for measuring the degree of morphological maturation, application of this method to geological sands (sandstones) may enable estimation of the ancient morphological maturation and ancient physical energy during the transportation of sands in a given environment.

However, it can also be expected that fluvial sands mature as downstream distance increases, but such a relation was not observed for either of the fluvial systems (FL1 and FL2). It is likely that the rivers investigated have drainage distances which are too short to show downstream sediment maturation (Yagishita *et al.*, 2000).

Meanwhile, glacial sediments are dislocated from this continuous linear trend in SEF and REF1, and define a peculiar maturity trend caused by the grinding or plucking of grains beneath ice, except for one sample collected from the Athabasca Glacier (G2-1). One exceptional glacial sample collected from the Athabasca Glacier deviates from the glacial domain,

and belongs to the maturity trend of the fluvial–foreshore–aeolian alignment (G2-1), but the use of the SEF–REF1 diagram may enable the transportation histories of sedimentary grains to be evaluated.

CONCLUSION

The inherent problem in the application of the Fourier technique to grain shape analysis is the numerous descriptors that are generated by the technique, making comprehensive interpretations of the data difficult (Boggs, 2009). Rohlf & Archie (1984) and Iwata *et al.* (1998) showed that this problem can be overcome by combining elliptic Fourier analysis with principal component analysis (EF–PCA). Suzuki *et al.* (2013) demonstrated that this approach is also useful in the analysis of detrital grains. However, the normal use of elliptic Fourier and principal component analysis can depict only the macroscopic forms of grains (for example, elongated or spherical), and the method is unable to depict microscopic grain shape characteristics (for example, surface smoothness). An elliptic Fourier and principal component analysis approach based on both the variance–covariance matrix and the correlation matrix enabled extraction of both the macroscopic form of grains (REF1) as well as microscopic surface smoothness (standardized elliptic Fourier). The REF1 and standardized elliptic Fourier indices discriminate sand grains derived from glacial, fluvial, foreshore and aeolian environments. One potential application of the REF1 and standardized elliptic Fourier indices is discrimination of ancient depositional environment or wave power of geological sedimentary records. However, in order to assess the reliability of the standardized elliptic Fourier and REF1 indices as tools for the discrimination of palaeo-sedimentary environments, additional work will be required.

ACKNOWLEDGEMENTS

The authors are indebted to the Chief Editor Dr Stephen Rice and the reviewer Dr Daniel Buscombe for their help improving the earlier manuscript. We also thank Dr. Kazuyoshi Moriya of Kanazawa University for assisting our fieldwork in Canada. We also thank Parks Canada for giving us permission to sample the Athabasca glacial sands.

REFERENCES

Anderson, R.S. (1986) Erosion profiles due to particles entrained by wind: application of an eolian sediment-transport model. *Geol. Soc. Am. Bull.*, **97**, 1270–1278.

Barclay, D.R. and **Buckingham, M.J.** (2009) On the shapes of natural sand grains. *J. Geophys. Res.*, **114**, B02209.

Bernasconi, S.M and BigLink Project Members (2008) Weathering, soil formation and initial ecosystem evolution on a glacier forfield: a case study from the Damma Glacier, Switzerland. *Mineral. Mag.*, **72**, 19–22.

Blott, S.J. and **Pye, K.** (2008) Particle shape: a review and new methods of characterization and classification. *Sedimentology*, **55**, 31–63.

Boggs, S., Jr (2009) *Petrology of Sedimentary Rocks*. Cambridge University Press, Cambridge, 600 pp.

Bohrer, R. (1967) On sharpening Scheffe bounds. *J. Roy. Stat. Soc. Ser. B*, **29**, 110–114.

Brown, P.J., **Ehrlich, R.** and **Colquhoun, D.J.** (1980) Origin of patterns of quartz sand types on the Southeastern United States continental shelf and implications on contemporary shelf sedimentation – Fourier grain shape analysis. *J. Sed. Petrol.*, **50**, 1095–1100.

Cox, E.P. (1927) A method of assigning numerical and percentage values to the degree of roundness of sand grains. *J. Paleontol.*, **1**, 179–183.

Diepenbroek, M., **Bartholoma, A.** and **Ibbeken, H.** (1992) How round in round? A new approach to the topic 'roundness' by Fourier grain shape analysis. *Sedimentology*, **39**, 411–422.

Dowdeswell, J.A. (1982) Scanning electron micrographs of quartz sand grains from cold environments examined using Fourier shape analysis. *J. Sed. Petrol.*, **52**, 1315–1323.

Ehrich, R., **Brown, P.J.**, **Yarus, J.M.** and **Przygocki, R.S.** (1980) The origin of shape frequency distributions and the relationship between size and shape. *J. Sed. Petrol.*, **50**, 475–484.

Ehrlich, R. and **Weinberg, B.** (1970) An exact method for characterization of grain shape. *J. Sed. Res.*, **40**, 205–211.

Freeman, H. (1974) Computer processing of line drawing images. *Comp. Surv.*, **6**, 57–97.

Hentschel, M.L. and **Page, N.W.** (2003) Selection of descriptors for particle shape characterization. *Part. Part. Syst. Charact.*, **20**, 25–38.

Hudson, C.B. and **Ehrlich, R.** (1980) Determination of relative provenance contributions in samples of quartz sand using Q-mode factor analysis of Fourier grain shape data. *J. Sed. Petrol.*, **50**, 1101–1110.

Iwata, H. and **Ukai, Y.** (2002) SHAPE: a computer program package for quantitative evaluation of biological shapes based on elliptic Fourier descriptors. *J. Heredity*, **93**, 384–385.

Iwata, H., **Niikura, S.**, **Matsuura, S.**, **Takano, Y.** and **Ukai, Y.** (1998) Evaluation of variation of root shape of Japanese radish (*Raphanus sativus* L.) based on image analysis using Fourier descriptors. *Euphytica*, **102**, 143–149.

Jerolmack, D.J. and **Brzinski, T.A.** (2010) Equivalence of abrupt grain-size transitions in alluvial rivers and eolian sand seas: a hypothesis. *Geology*, **38**, 719–722.

Keddy, P.A. (1982) Quantifying within-lake gradients of wave energy: interrelationships of wave energy, substrate particle size and shoreline plants in Axe Lake, Ontario. *Aquat. Bot.*, **14**, 41–58.

Kennedy, S.K. and **Lin, W.H.** (1992) A comparison of Fourier and fractal techniques in the analysis of closed forms. *J. Sed. Petrol.*, **62**, 842–848.

Krumbein, W.C. (1941) Measurement and geological significance of shape and roundness of sedimentary particles. *J. Sed. Petrol.*, **11**, 64–71.

Kuhl, F.P. and **Giardina, C.R.** (1982) Elliptic Fourier features of a closed contour. *Comput. Graph. Image Process.*, **18**, 236–258.

Lees, G. (1964) A new method for determining the angularity of particles. *Sedimentology*, **3**, 2–21.

Livsey, D.N., **Simms, A.R.**, **Clary, W.G.**, **Wellner, J.S.**, **Anderson, J.B.** and **Chandler, J.P.** (2013) Fourier grain-shape analysis of Antarctic marine core: the relative influence of province and glacial activity on grain shape. *J. Sed. Res.*, **83**, 80–90.

Luckman, B.H. (1988) Dating the moraines and recession of Athabasca and Dome Glaciers, Alberta, Canada. *Arctic Alpine Res.*, **20**, 40–54.

Mazzullo, J. and **Magenheimer, S.** (1987) The original shapes of quartz sand grains. *J. Sed. Petrol.*, **57**, 479–487.

Pye, K. and **Mazzullo, J.** (1994) Effects of tropical weathering on quartz grain shape: an example from Northeastern Australia. *J. Sed. Res.*, **A64**, 500–507.

Rajaei, M., **Poorbagher, H.**, **Farahmand, H.**, **Mortazavi, M.S.** and **Eagderi, S.** (2014) Interpopulation differences in shell forms of the pearl oyster, *Pinctada imbricata radiata* (Bivalvia: Pterioida), in the northern Persian Gulf inferred from principal component analysis and elliptic Fourier analysis. *Turk J. Zool.*, **38**, 42–48.

Rogers, J.W., **Krueger, W.C.** and **Krog, M.** (1963) Sizes of naturally abraded materials. *J. Sed. Petrol.*, **33**, 628–632.

Rohlf, F.J. and **Archie, J.W.** (1984) A comparison of Fourier methods for the description of wing shape in mosquitoes (Diptera: Culicidae). *Syst. Zool.*, **33**, 302–317.

Schwarcz, H.P. and **Shane, K.C.** (1969) Measurement of particle shape by Fourier analysis. *Sedimentology*, **13**, 213–231.

Suzuki, K., **Sakai, K.** and **Ohta, T.** (2013) Quantitative evaluation of grain shapes by utilizing Fourier and fractal analysis and implications for discriminating sedimentary environments. *J. Geol. Soc. Japan*, **119**, 205–216 (in Japanese with English abstract).

Tafesse, S., **Fernlund, J.M.R.**, **Sun, W.** and **Bergholm, F.** (2013) Evaluation of image analysis methods used for quantification of particle angularity. *Sedimentology*, **60**, 1100–1110.

Thomas, M.C., **Wiltshire, R.J.** and **Williams, A.T.** (1995) The use of Fourier descriptors in the classification of particle shape. *Sedimentology*, **42**, 635–645.

Tracey, S.R., **Lyle, J.M.** and **Duhamel, G.** (2006) Application of elliptical Fourier analysis of otolith form as a tool for stock identification. *Fish. Res.*, **77**, 138–147.

Tysmans, D., **Claeys, P.**, **Deriemaeker, L.**, **Maes, D.**, **Finsy, R.** and **van Molle, M.** (2006) Size and shape analysis of sedimentary grains by automated dynamic image analysis. *Part. Part. Syst. Charact.*, **23**, 381–387.

Wadell, H. (1932) Volume, shape, and roundness of rock particles. *J. Geol.*, **40**, 443–451.

Wadell, H. (1933) Sphericity and roundness of rock particles. *J. Geol.*, **41**, 310–331.

Wentworth, C.K. (1919) A laboratory and field study of cobble abrasion. *J. Geol.*, **27**, 507–521.

Yagishita, K., **Nirasawa, M.**, **Saito, K.** and **Terui, K.** (2000) Compositional characteristics of Holocene sands in a mature magmatic arc belt: a case study of river sands derived from plutonic and accretionary complexes, northeast Japan. *Mem. Geol. Soc. Japan*, **57**, 19–28 (in Japanese with English abstract).

Yoshioka, Y., **Iwata, H.**, **Ohsawa, R.** and **Ninomiya, S.** (2004) Analysis of petal shape variation of *Primula sieboldii* by elliptic Fourier descriptors and principal component analysis. *Ann. Bot.*, **94**, 657–664.

Manuscript received 30 January 2014; revision accepted 11 December 2014

Supporting Information

Additional Supporting Information may be found in the online version of this article:

Data S1. Supporting information.